

Article

Fabrication and Characterization of Free-Standing and Flexible Polyaniline Membranes: Role of Graphene Nanoscrolls

Rauf Mahmudzade * and Dilip Depan * 

Chemical Engineering Department, Institute for Materials Research and Innovation,
University of Louisiana at Lafayette, P.O. Box 44130, Lafayette, LA 70504-4130, USA

* Correspondence: rauf.mahmudzade@gmail.com (R.M.); ddepan@louisiana.edu (D.D.)

Abstract: Wearable technologies can contribute to the early and accurate detection of chronic diseases which can be achieved by the integration of biosensors into wearable technologies. However, the challenges associated with the performance of current electrode materials—i.e., flexibility, conductivity, and mechanical stability, made from conducting polymers are preventing their widespread usage. Herein, we report a freestanding and flexible electrode synthesized from polyaniline (PANI) and graphene nanoscrolls (GNS). The PANI-GNS nanohybrid membranes were synthesized via chemical oxidative polymerization and characterized by scanning electron microscopy (SEM), Fourier transform infrared spectroscopy (FTIR), nanoindentation (NI), and four-point probe techniques. FTIR results showed an increase in conjugation length of the PANI after the addition of GNS into the mixture which can be indicative of an enhancement of electrical properties. Nanoindentation studies showed an elastic modulus and hardness of 2.6 GPa and 0.17 GPa, respectively, for PANI-GNS-5 nanocomposite, compared to 1.9 GPa and 0.08 GPa, for pure PANI. This was later confirmed by the four-point probe technique as the addition of GNS increased the conductivity of electrodes up to 9 S/cm at a 5% weight ratio. Moreover, SEM results of the PANI-GNS showed an open porous morphology of the polymer matrix in comparison with pure PANI samples which would readily translate into higher amounts of enzyme immobilization on the surface.

Keywords: nanoindentation; FTIR; conducting polymers; graphene nanoscrolls



Citation: Mahmudzade, R.; Depan, D. Fabrication and Characterization of Free-Standing and Flexible Polyaniline Membranes: Role of Graphene Nanoscrolls. *Macromol* **2022**, *2*, 543–553. <https://doi.org/10.3390/macromol2040035>

Academic Editor: Ana María Díez-Pascual

Received: 18 July 2022

Accepted: 15 November 2022

Published: 21 November 2022

Publisher's Note: MDPI stays neutral with regard to jurisdictional claims in published maps and institutional affiliations.



Copyright: © 2022 by the authors. Licensee MDPI, Basel, Switzerland. This article is an open access article distributed under the terms and conditions of the Creative Commons Attribution (CC BY) license (<https://creativecommons.org/licenses/by/4.0/>).

1. Introduction

Amperometric devices and materials have attracted tremendous attention due to their wide applications as semiconductors, super-capacitors, and flexible electrodes [1]. Utilization of conducting polymers as amperometric materials solves the problems such as poor stability and slower response rate, which is associated with inorganic materials.

Conducting polymers have been utilized to fabricate amperometric devices since their unique electroactive properties allow them to act as excellent substrates for the immobilization of biomolecules and rapid transfer of electrons [2]. Polyaniline (PANI) among various conducting polymers is particularly attractive due to its high surface area for enzyme immobilization, high specific capacitance and good environmental stability [3]. Moreover, it provides a suitable matrix for enzyme immobilization that significantly enhances the electrical signals by acting as a mediator for electron transfer during enzymatic reactions. However, the utilization of polyaniline has been limited because of its poor solubility, processability, and mechanical properties [4]. Thus, extensive efforts have been directed toward overcoming the challenges associated with the fabrication of polyaniline-based electrodes. For instance, Dawu et al. fabricated a PANI-based ammonia (NH₃) sensor that offers potential applications in smart devices [5]. However, the short life cycle with repeated use and low charge transfer capability poses challenges in the wide usage of PANI. Studies have shown that the electrical conductivity and long-term mechanical stability of the material can be improved by an order of magnitude with the addition of nanomaterials

into the PANI matrix [6]. Studies have shown that signal to noise ratio of the intended wearable devices can be significantly enhanced if the conformal contact between the device and the tissue is established. However, the rigidity and bulkiness of conventional biosensors manifest a mismatch between the material properties and intended applications, hindering their use on the soft and hierarchically textured, and curvilinear surfaces of the human body [7].

Graphene nanoscrolls (GNS) is a one-dimensional open-ended tubular structure consisting of tubular layers of graphene sheets formed by rolling in a continuous manner. GNS possesses superior structural stability that provides it with the capability to overcome non-uniform dispersion and poor adhesion of their planar and tubular counterparts [8]. Additionally, the continuity of a rolled-up graphene sheet provides a uniform response with superior mechanical, thermal, and electrical properties. The open ends and tunable interlayer surface allow for solvent and biomolecule accessibility just by facile infiltration [9]. Nanohybrid membranes of PANI with carbon-based nanomaterials such as graphene nanoplatelets (GNPs) and carbon nanotubes (CNTs) usually follows in-situ polymerization over these nanomaterials. However, the synthetic approaches generally provides either insoluble powders or rigid non-flexible membranes, thus limiting its applications. Recently, GNS has been used to prepare high performance supercapacitors with PANI [10]. However, the conducting and nanomechanical properties, which are detrimental in wearable devices have never been reported.

In the present work, a new flexible free-standing membrane of PANI-GNS nanocomposite films were formed during a chemically oxidative process involving in situ polymerization of aniline. Several characterization techniques—i.e., FTIR, SEM, XRD, nanoindentation, and four-point probe technique were employed to evaluate the chemical, mechanical and electrical properties of the synthesized composite. Moreover, the electrical properties of the PANI-GNS composite were comparatively analyzed with that of the carbon nanotubes and graphene nanoplatelets.

2. Materials and Methods

2.1. Materials

All chemicals used in this work were of analytical grade. Aniline (ANI), ammonium persulfate (APS), ammonia solution (28–30%), hydrochloric acid (HCl, 35–38%), Camphor-sulfonic acid (CSA), and N-Methyl-2-pyrrolidone (NMP), were all received from Fisher Scientific, Waltham, MA, USA. The aniline was distilled under reduced pressure before use, while other chemicals were used as received. Type X-S, lyophilized powder of Glucose Oxidase with 100,000–250,000 units/g solid (without added oxygen) were acquired from Sigma-Aldrich, Burlington, MA, USA. Graphene nanoplatelet (GNP) powder, with an average of five to seven atomic layers of 2D graphite layers and toluene (purity greater than or equal to 99.5%), were also received from Sigma-Aldrich, USA.

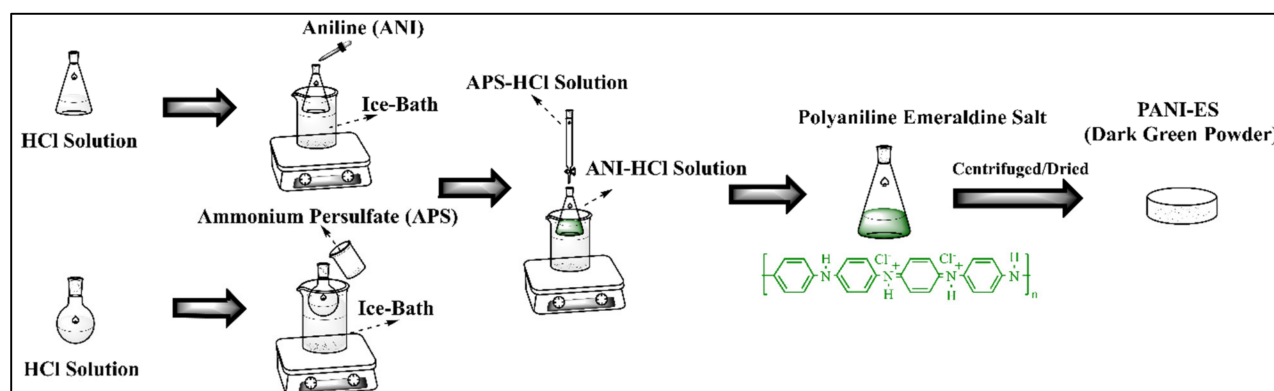
2.2. Conversion of Graphene Nanoplatelets (GNPs) to Graphene Nanoscrolls (GNS)

GNSs were synthesized using a previously reported methodology in which GNPs were employed as precursor [9]. 2.0 mg of GNPs was added to 20 mL of toluene and sonicated using a SONICS Vibra-Cell ultrasonic liquid processor with an amplitude of 40%. Having applied ultrasonication at 2-minute intervals, three times for a total of 6 min, the GNP-toluene mixture was dispersed into liquid nitrogen (approximately 1 L) in a mortar. Solid particles of toluene were allowed to melt at room temperature and then transferred to a petri dish for the solvent to evaporate overnight, thereby obtaining GNS.

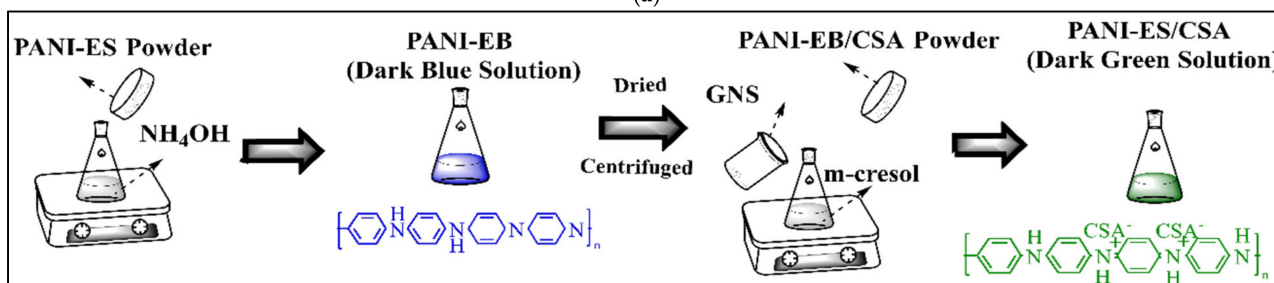
2.3. PANI-GNS Flexible Film Preparation

1 mL of ANI and 2.5 g of APS were added to 90 and 100 mL of 1 M HCl, respectively, both of which were carried out in an ice bath. Polyaniline in the emeraldine salt form (PANI-ES) was synthesized by dropwise addition of APS-HCl mixture into ANI-HCl solution with

constant stirring at 0–5 °C for 6–8 h. The collected dark-green PANI powder was washed several times with alcohol and water to remove the contamination [10] [Scheme 1a].



(a)



(b)

Scheme 1. (a) Oxidative polymerization of aniline with ammonium persulfate in acidic environment. (b) Redoping of polyaniline emeraldine salt with camphorsulfonic acid.

Afterward, to de-dope the emeraldine salt powder, it was added into a 0.1 M ammonia solution with continuous stirring for 24 h at room temperature followed by a second wash with alcohol and water several times. PANI-EB was dried under vacuum for 8 h at 60 °C. To achieve better electrical conductivity, the PANI was re-doped using CSA as reported elsewhere [10]. Then the CSA-doped PANI was added into the m-cresol/chloroform mixture with constant stirring for 24 h, thus forming a dark green colored solution. To synthesize PANI-GNS films, GNS with different weight fractions (1, 2.5, 5 wt. %) were added into the as-obtained dark-green solution, followed by 1 h stirring and 1 h ultrasonic treatment, respectively [Scheme 1b].

Then, the mixed solution was cast on glass substrates and dried at 80 °C on a hot plate for 24 h to form flexible and free-standing electrodes, which can be easily peeled off from the substrate. These films were abbreviated as PANI, PANI-GNS-1, PANI-GNS-2.5, and PANI-GNS-5, respectively.

2.4. Immobilization of Glucose Oxidase on Flexible Electrode

Fresh solutions of glucose oxidase were prepared by dissolving GOx (10 mg/mL) in a 0.02 M PBS solution and stored at 4 °C. Then, 15 µL of the GOx solution was deposited onto each surface of the free-standing electrodes. The electrode was maintained under ambient conditions to completely dry. Afterward, the immobilization of GOx on the surface of the PANI-GNS films was achieved by cross-linking through glutaraldehyde [11]. A total of 15 µL of 0.1% glutaraldehyde was added onto the electrode in a similar fashion to GOx and allowed to react for 4 h to cross-link the GOx with the PANI and PANI-GNS electrodes. Formed PANI-GOx and PANI-GNS-GOx electrodes were rinsed thoroughly with PBS solution and stored at 4 °C when not in use.

2.5. Characterization

2.5.1. Scanning Electron Microscopy: Morphological Analysis

The surface morphology of the samples was investigated using scanning electron microscope (Scios 2 DualBeam FIB/SEM) at an accelerating voltage of 5 kV. The samples were mounted on an aluminum stub and sputter-coated with a 10 nm layer of gold, before imaging.

2.5.2. Fourier Transform Infrared Spectroscopy: Chemical Analysis

The attenuated total reflectance Fourier transform infrared spectrometer (ATR-FTIR, Bruker LUMOS II) was used to determine the changes in the chemical structure of EPON-IPD samples with the exposure to UV radiation. An average of 32 spectra were recorded within the test range of 4000–500 cm^{-1} with 4 cm^{-1} resolution. Subsequent spectral processing techniques involved baseline and atmospheric corrections.

2.5.3. Nanoindentation: Modulus and Hardness Studies

Nanoindenter G-200 from MTS equipped with Berkovich tips was used to measure the mechanical properties of the samples up to 10 microns. The operational specifications of the nanoindenter were as follows: load range is 0.4 to 500 mN, displacement resolution was less than 0.01 nm, and the load resolution is 50 nN. Continuous stiffness measurement method (CSM) which is a suitable method for polymeric samples was utilized to drive the raw data and analyzed further. 15 indentations were conducted at random locations, and average and standard deviations were reported to acquire reliable data.

2.5.4. Four-Point Probe Technique: Resistivity and Conductivity Studies

Four-point probe system FPP5000 from Veeco was used to measure the direct current resistivity and electrical conductivities of CSA doped PANI nanocomposites in the absence and presence of nanomaterials. Nanocomposites were fixed on silicon wafer substrates using double-sided tape and measurements were conducted at room temperature. An average of 5 conductivity measurement was conducted for each electrode.

2.5.5. X-ray Diffraction

X-ray diffraction (XRD) was used to determine the d-spacing and the percent crystallinity of each of the samples. The measurements were carried out in a MiniFlex 600 from Rigaku Americas Corporation. The full width half maximum (FWHM) values were also determined as well as the intensities of the peaks. The samples were measured over a 2θ range of 10–50°, at a scan rate of 5°/minute with $\text{CuK}\alpha$ ($\lambda = 0.154$ nm) radiation. Further, XRD analysis was also conducted to determine the d-spacing, crystallite size, and full width at half maximum (FWHM) using Bragg's and Scherrer's equations [12].

3. Results and Discussion

3.1. Preparation of Flexible Electrode

In this study, PANI was selected as the primary conducting polymer matrix for the fabrication of flexible electrodes. Unlike previously reported methodology, we employed an ex-situ synthesis of PANI/GNS nanocomposites. Moreover, PANI was re-doped with CSA to further increase the electrical properties [13]. For this purpose, the only conductive state of polyaniline—i.e., half-oxidized emeraldine salt form (ES) was synthesized via chemical oxidative polymerization of aniline monomer in an acidic environment by adding ammonium persulfate (APS) as the oxidizing agent. The use of APS enables the elimination of a proton from the ANI monomer and the initiation of the polymerization by redox processes involving the repetition of monomeric units. It is critical to determine the proper ANI/APS ratio which, in our case, was 1:1 to obtain the optimum equilibrium between yield and electrical conductivity parameters [14]. As can be observed from Scheme 1a, the reaction must be conducted at low temperatures (0–5 °C), due to the nature of the polymerization reaction being exothermic. Afterward, PANI was converted from emeraldine salt to emeraldine base (EB) form using a redox agent—i.e., ammonium

hydroxide (NH_4OH) for the secondary doping process with camphorsulfonic acid (CSA). According to Cho et al., secondary doping with CSA changes the PANI structure from compact to expanded coils which promote electron delocalization and result in improved conductivity of two/three orders of magnitude compared to conventional pure PANI electrodes [15].

However, the movement of CSA molecules within the *m*-cresol solution can be suppressed due to the strong hydrogen bonding which can slow down the doping at nitrogen bonded quinone diamine segment [15]. Thus, as provided in Scheme 1b, a co-solvent system of *m*-cresol/chloroform (CHCl_3) ($v/v = 4:1$) is utilized to promote the diffusion of CSA for dissolution of the PANI/CSA powders. For the synthesis of electrodes, GNS were also added to the system in this step. Through this methodology, highly viscous PANI-GNS samples re-doped with CSA within *m*-cresol/chloroform solution were obtained. Notably, higher viscosity is associated with increased hydrodynamic volume and rapid changes in the molecular conformation of PANI/CSA from a compact coil to an expanded coil [16]. Consequently, the *m*-cresol/chloroform co-solvent system was required to obtain highly conductive PANI-GNS electrodes (Figure 1).

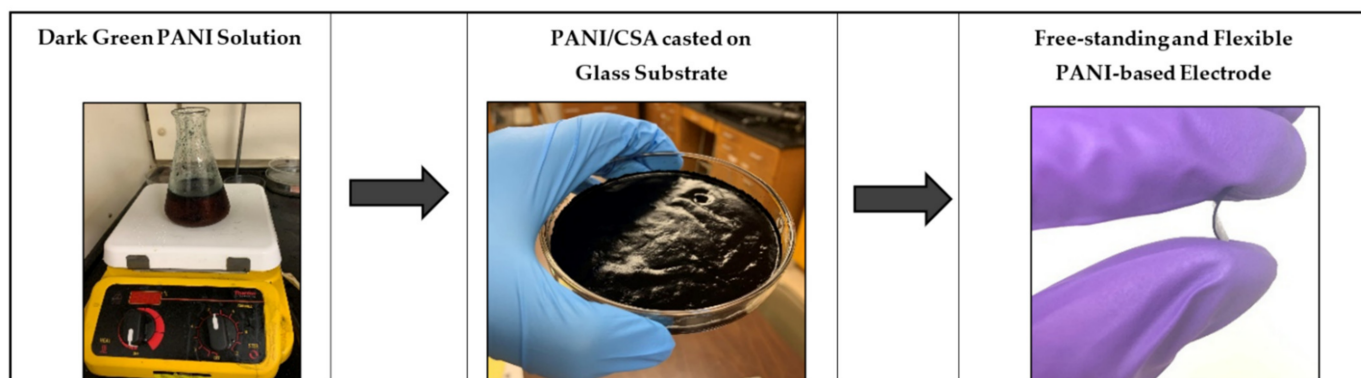


Figure 1. Optical images of the fabrication of flexible and free-standing PANI/CSA electrode.

GOx immobilization was achieved by drop-casting, which produces a glucose biosensor with the GOx directly attached to the high surface area of PANI and PANI-GNS electrodes, following a crosslinking procedure using glutaraldehyde [17]. Through the provided methodology, flexible and free-standing PANI-based films without any binders or additives were prepared which has been a long-standing challenge that prevents the widespread use of this material for the fabrication of biosensors [18]. Moreover, the conductivity of the electrode material and performance parameters of the conducting membranes was significantly enhanced by secondary doping as well as the addition of GNS into the polymer matrix which was utilized for the first time for the intended applications in literature according to our knowledge [19].

3.2. Spectroscopic Analysis

FTIR spectroscopy was used to investigate the functional group formation in CSA doped PANI and PANI-GNS nanocomposites, before and after enzyme immobilization [Figure 2]. Pure PANI showed the characteristic peaks at 1556 and 1475 cm^{-1} , which are attributed to stretching vibrations of $\text{C}=\text{N}$ in quinone diamine segment and $\text{C}=\text{C}$ stretching of benzenoid rings, respectively [20]. The wavenumbers of these two primary peaks were lower than those provided in literature for PANI in emeraldine salt form [21].

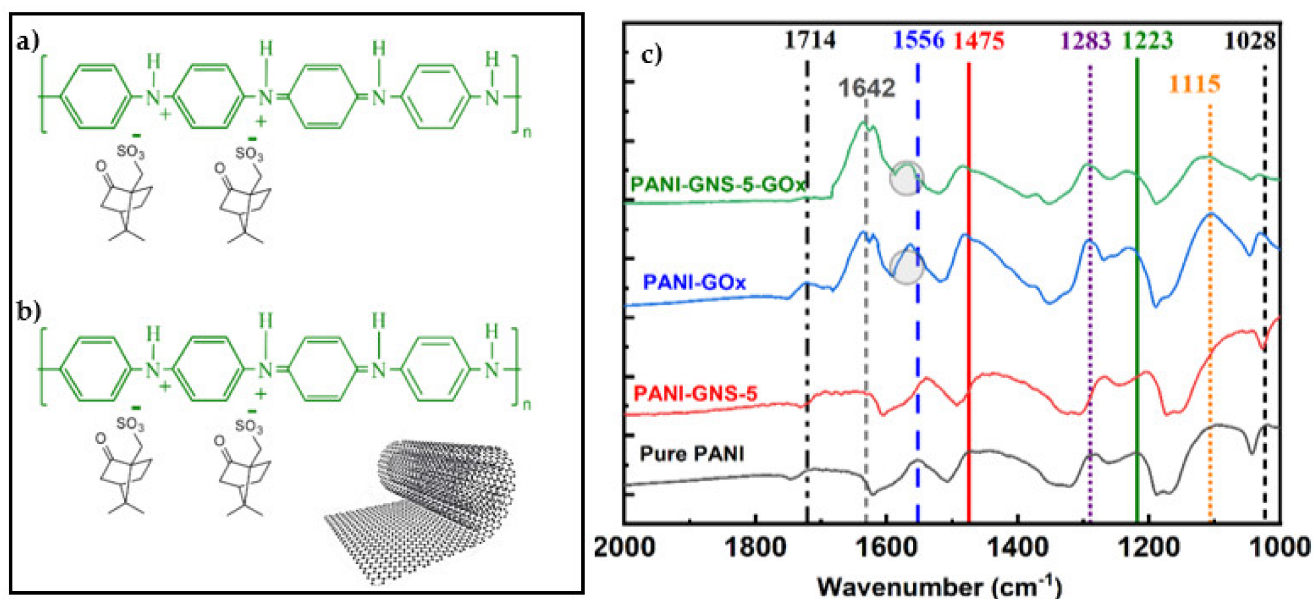


Figure 2. Chemical structure of CSA-doped (a) PANI, (b) PANI-GNS; (c) FTIR Spectra of PANI, PANI-GNS-5, PANI-GOx, and PANI-GNS-5-GOx samples.

Consistent with the molecular structures provided in Scheme 1a,b, this blue shift in our samples was explained by the restricted vibrational motion of polymer chains which was the result of the development of polaron structures in the PANI-ES form due to the secondary redoping with big counter ions of CSA [15,21]. Pure PANI also showed the characteristic C-N stretching in benzenoid unit (1283 and 1223 cm^{-1}) and aromatic C-H in-plane bending (1115 cm^{-1}) bands (Figure 2c). Additionally, the stretching vibrations around 1714 cm^{-1} (carbonyl group) and 1028 cm^{-1} (sulfonic group) confirmed successful redoping of the PANI with CSA [22].

Among GNS incorporated electrodes, PANI-GNS-5 nanocomposite showed the most significant differences in terms of spectral alterations. Comparing the FTIR spectra of PANI-GNS-5 with pure PANI, it was observed that the interaction between graphitic materials and polymer chains manifested themselves by peak shifts and intensity increases. Compared with the pure PANI sample, the C=C stretching vibration band of the quinoid and benzenoid rings in PANI-GNS is red-shifted from 1556 and 1475 cm^{-1} to lower wavenumbers—i.e., 1538 and 1455 cm^{-1} , respectively. This indicates that PANI-GNS nanocomposites involve higher degrees of conjugation which can originate from conjugational π - π interactions between nanoscrolls and polymer chains [23,24]. According to Liu et al., the increase in conjugation length and electron delocalization can lead to enhanced conductivity of polymer chains which will be confirmed by four-point probe resistivity measurements [25] (Section 3.5).

The incorporation of GOx into the PANI and PANI-GNS matrix can be confirmed by analyzing the amide IR bands which are widely used for the monitoring of conformational changes in proteins. As provided in Figure 2, unlike pure PANI and PANI-GNS electrodes, two amide bands, within the ranges of 1700~1600 cm^{-1} (amide I) and 1600~1500 (amide II) were observed for GOx immobilized specimens. The amide I band around 1642 cm^{-1} was attributed to C=O stretching vibrations of peptide linkages in the glucose oxidase backbone. The latter—i.e., amide II at 1574 cm^{-1} was assigned to a combination of N-H in-plane bending and C-N stretching of the peptide groups [26]. However, amide II bands were overlapping with that of characteristic PANI peaks as can be seen from the blue shift towards higher wavelength for both pure PANI and PANI-GNS samples.

3.3. Morphological Analysis

Scanning electron microscope images of pure polyaniline sample possessed the most uniform and smooth surface among all other electrodes without any pores or particle inclusions [Figure 3a]. This was indicative of good solubility in m-cresol/chloroform solution which was required to achieve higher electrical conductivity [27].

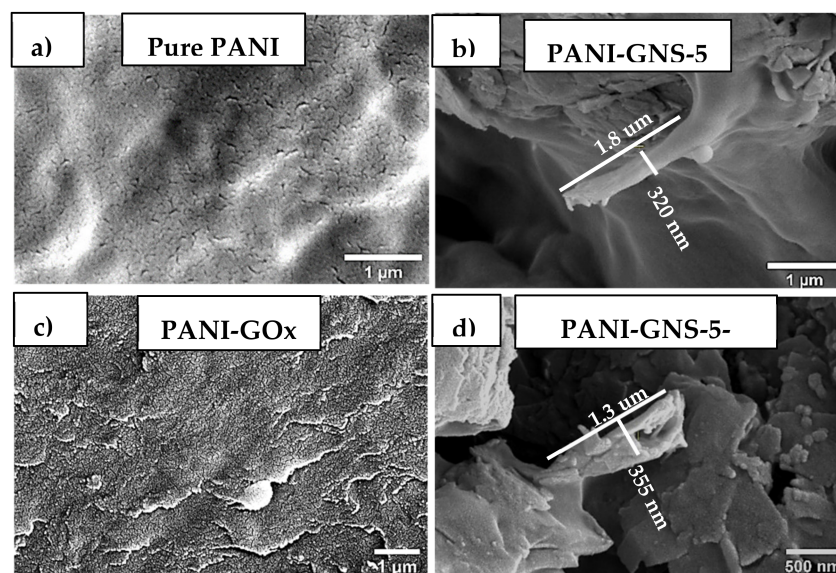


Figure 3. Surface morphology of (a) PANI, (b) PANI-GNS-5, (c) PANI-GOx, and (d) PANI-GNS-5-GOx electrodes; single fiber of graphene nanoscrolls from (b) PANI-GNS-5 and (d) PANI-GNS-5-GOx.

GNS with lengths and diameters in the range of a few micrometers and 300–500 nm, respectively, can be envisaged as rigid macromolecules with rolled-over graphite sheets which give rise to the formation of macro-pores and surface cracks [Figure 3b] through which the analyte molecules can easily diffuse into the electrode. SEM and TEM images of pure GNS are given in Supplementary Materials Figure S1. Figure 3c,d show the surface of PANI and PANI-GNS-5 electrodes after the immobilization of GOx, confirmed by the appearance of granular morphology. Achieving a higher amount of GOx immobilized on the surface is more favorable as it would enable enhanced analyte detection as well as electron transfer. In the latter case more GOx is embedded deeper into the nanocomposite, bonding fibers, and agglomerates to each other, which makes the surface more favorable for the entrapment of enzyme molecules. Similarly, Peng et al. also confirmed that the quantity of enzyme immobilized on electrode surface can be significantly increased due to the open and spiral structure of rolled graphene sheets [28–30]. Combined with the interlayer spaces and channels of scrolled structures, open surface morphology achieved by GNS incorporation into PANI matrix can facilitate the mass transport of analyte molecules leading to more exposed active sites within nanocomposite, thus improving the overall performance of the electrodes. Figure S2 presents the SEM images of PANI-GNS-1, PANI-GNS-2.5, and PANI-GNS-5, illustrating the open porous yet rough surface texture that might be critical in the immobilization of GOx.

3.4. Mechanical Analysis

Micro-mechanical properties of CSA doped PANI films at different GNS loadings were analyzed using nanoindentation studies. The elastic modulus (E) and hardness (H) of the nanohybrid membranes were derived by using Oliver and Pharr's method derived from load-displacement curves [31]. As can be observed from Figure 4, the addition of GNS into the PANI matrix improved elastic modulus and hardness to 2.6 GPa and 0.17 GPa, respectively, for PANI-GNS-5 nanocomposite, compared to 1.9 GPa and 0.08 GPa, for pure PANI.

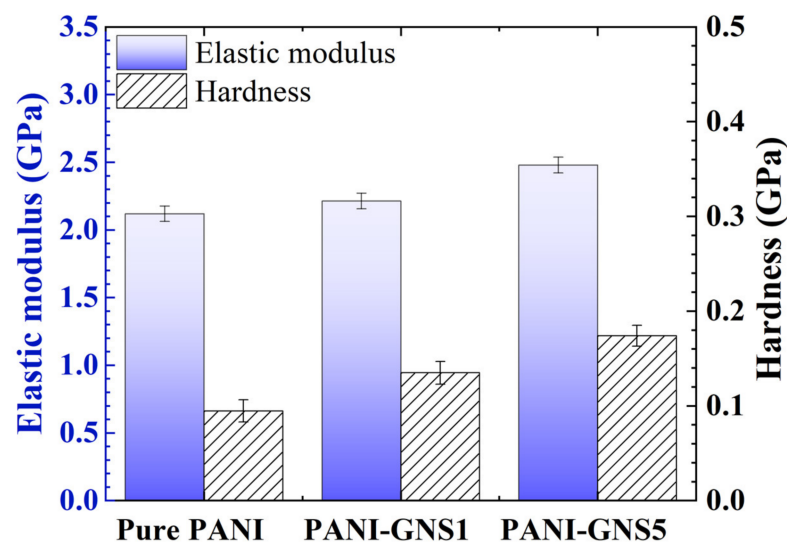


Figure 4. Young modulus and hardness of flexible and free-standing PANI/CSA membranes at various GNS content.

This higher resistance against the penetration of the indenter probe can be attributed to the interaction between closely packed PANI chains due to large CSA molecules and graphene nanoscrolls [15,16]. The superior adhesion behavior of graphene nanoscrolls owing to its strain generated during the scrolling process of nanoplatelets has been reported in previous studies [32]. Results suggest that the increase of 0.74 GPa and 0.08 GPa in respective nanocomposite modulus and hardness with increasing GNS content was the result of restricted movement of polymer chains due to big CSA counter ions as well as strong adhesion of nanoscrolls resulting in better mechanical interlocking. Chen et al., in a recent study, studied the presence of a correlation between elasticity and conductivity of functionalized PANI films. It has been reported that the most significant charge carrier mobility was achieved at maximum values of elastic modulus due to the enhanced structural order in polymer chain packing and alignment [33]. Thus, it is to be expected that CSA doped PANI electrodes with the highest amount of GNS content would demonstrate better conductivity which will be investigated using the four-point probe technique. Further, XRD data (Figure S3 and Table S1) reveals the XRD patterns of pure PANI and its GNS loaded membranes. The decrease in full width at half-maximum (FWHM) in nanohybrid samples is an indication of ordering of PANI macromolecular chains. Similarly, modulus and hardness data (Figure S4) as obtained by nanoindentation confirm that the mechanical integrity of the samples did not get affected after conductivity tests.

3.5. Conductivity Analysis

Sheet resistivity and the conductivity of CSA doped PANI electrodes at different GNS content were measured using the **four-point probe** technique. As can be observed from Figure 5a, the electrical conductivity of the nanocomposites improved from 3 S/cm to 9 S/cm when the GNS ratio was increased from 0 to 5%. The increase in electrical conductivity of the fabricated electrodes was attributed to the “conducting bridge” effect of GNS which creates electrically active junction points [34]. Higher charge carrier mobility achieved due to enhanced structural order in polymer chain packing was the result of restricted polymer chain movements due to big CSA counter ions and superior adhesion properties of GNS [15,16]. The presence of intrinsically conductive GNS provides additional routes for charge transport as opposed to discontinuous electron pathways in the case of only pure PANI chains. Moreover, strong π - π conjugation between PANI and GNS contributes to the formation of a rigid film structure in such a way that the conducting π electrons can easily hop between polymer backbones, thus improve film conductivity [35–37].

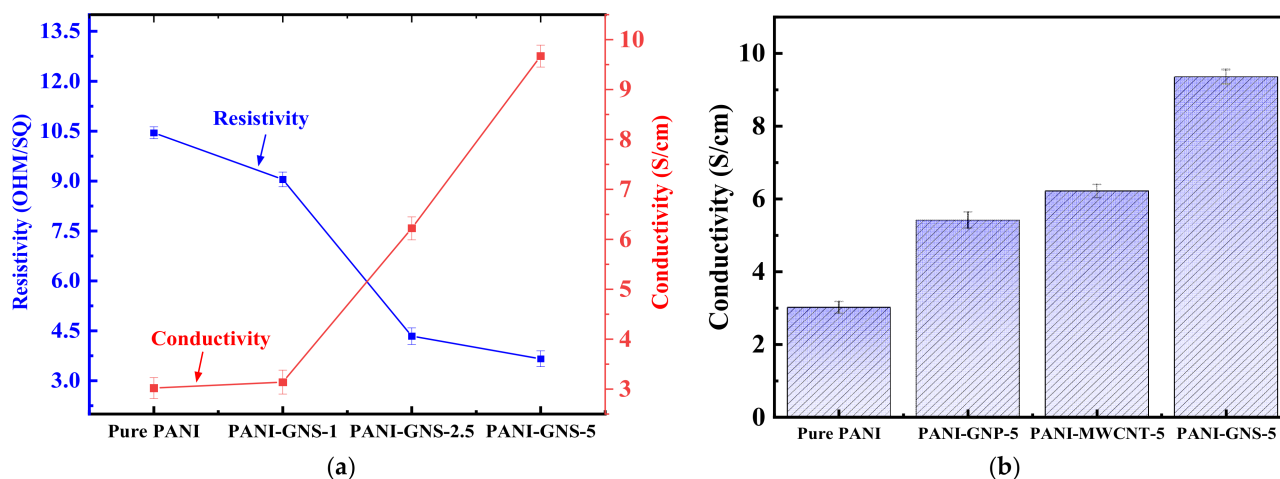


Figure 5. Electrical properties of PANI/CSA electrodes (a) at different GNS content, (b) in presence of different nanomaterials.

The effects of different nanomaterials—i.e., multiwalled carbon nanotubes (MWCNT) and graphene nanoplatelets (GNP) on electrical properties of CSA-doped PANI were also studied. It was observed that incorporation of these carbon nanomaterials into polymer matrix increased the conductivity of electrodes to 5.4 S/cm and 6.3 S/cm in the case of GNP and MWCNT, respectively. However, it can be seen from Figure 5b, PANI-GNP nanocomposites yielded a lower conductivity value than PANI-MWCNT counterparts. This was consistent with the previous studies as graphene nanoplatelets lack the ability to form conductive networks in polymer matrices which would result in increased amounts of discontinued pathways for charge transport [37].

Additionally, the analysis of the conductivity properties of GNS yielded the highest value of 9 S/cm which was attributed to the structural continuity of the rolled-up one-graphene layer which lessens the effect of inter-wall tunneling interactions unlike the bamboo-like compartment structure of MWCNTs causing perturbations of electrical properties. The unique scrolled architecture of GNS was critical in achieving higher electrical conductivity as it provided additional routes for electron transfer and contributed to the formation of “conducting bridges”, minimizing the tunnelling effect at molecular level.

4. Conclusions

The PANI-GNS nanohybrid membranes were synthesized by chemical oxidative polymerization of aniline in the presence of APS as an oxidant. FTIR studies revealed successful incorporation of GNS into PANI matrix as well as the presence of higher degrees of conjugation which would result in better alignment of polymer chains. Moreover, morphological studies showed that the addition of the GNS into the polymer can alter the surface structure. Consistent with previously reported studies, the most significant charge carrier mobility of 9 S/cm was achieved at maximum values of elastic modulus (2.6 GPa) which belonged to PANI/CSA electrode with 5% GNS weight content due to the enhanced structural order in polymer chain packing which was confirmed via nanoindentation studies.

Supplementary Materials: The following supporting information can be downloaded at: <https://www.mdpi.com/article/10.3390/macromol2040035/s1>, Figure S1: Scanning and transmission electron micrographs of graphene nanoscrolls; Figure S2: (a–c) Scanning electron micrographs of PANI-GNS composites at various GNS content; Figure S3: X-ray diffraction (XRD) patterns of prepared flexible nanohybrid membranes; Figure S4: Elastic modulus and hardness values of pure PANI and GNS loaded nanohybrid membranes using nanoindentation; Table S1: Full width at half-maximum values of the prepared nanohybrid membranes.

Author Contributions: Conceptualization, R.M. and D.D.; methodology, R.M.; software, R.M.; validation, R.M., and D.D.; formal analysis, R.M.; investigation, R.M.; resources, D.D.; data curation, R.M.; writing—original draft preparation, R.M.; writing—review and editing, R.M. and D.D.; visualization, D.D.; supervision, D.D.; project administration, D.D.; funding acquisition, D.D. All authors have read and agreed to the published version of the manuscript.

Funding: This research was funded by the Louisiana Board of Regents grant: LEQSF (2020-21)-ENH-DE-20.

Institutional Review Board Statement: Not applicable.

Informed Consent Statement: Not applicable.

Conflicts of Interest: The authors declare no conflict of interest.

References

1. Kushwaha, C.S.; Singh, P.; Shukla, S.K.; Chemimi, M. Advances in conducting polymers nanocomposites based chemical sensors: An overview. *Mater. Sci. Eng. B* **2022**, *284*, 115856. [[CrossRef](#)]
2. Aydemir, N.; Malmström, J.; Travas-Sejdic, J. Conducting Polymer Based Electrochemical Biosensors. *Phys. Chem. Chem. Phys.* **2016**, *18*, 8264–8277. [[CrossRef](#)] [[PubMed](#)]
3. Lai, J.; Yi, Y.; Zhu, P.; Shen, J.; Wu, K.; Zhang, L.; Liu, J. Polyaniline-Based Glucose Biosensor: A Review. *J. Electroanal. Chem.* **2016**, *782*, 138–153. [[CrossRef](#)]
4. Gao, F.; Mu, J.; Bi, Z.; Wang, S.; Li, Z. Recent Advances of Polyaniline Composites in Anticorrosive Coatings: A Review. *Prog. Org. Coat.* **2021**, *151*, 106071. [[CrossRef](#)]
5. Lv, D.; Shen, W.; Chen, W.; Tan, R.; Xu, L.; Song, W. PSS-PANI-PVDF Composite based flexible NH₃-sensors with sub-PPm detection at room temperature. *Sens. Actuators B Chem.* **2021**, *328*, 129085. [[CrossRef](#)]
6. Cho, S.; Lee, J.S.; Joo, H. Recent Developments of the Solution-Processable and Highly Conductive Polyaniline Composites for Optical and Electrochemical Applications. *Polymers* **2019**, *11*, 1965. [[CrossRef](#)]
7. Xing, X.; Du, L.; Feng, D.; Wang, C.; Tian, Y.; Li, Z.; Liu, H.; Yang, D. Twistable and tailorable V₂O₅/PANI/GO nanocomposite textile for wearable ammonia sensing. *Sens. Actuators B Chem.* **2022**, *351*, 130944. [[CrossRef](#)]
8. Ajala, O.; Werther, C.; Nikaeen, P.; Singh, R.P.; Depan, D. Influence of Graphene Nanoscrolls on the Crystallization Behavior and Nano-mechanical Properties of Poly(lactic Acid). *Polym. Adv. Technol.* **2019**, *30*, 1825–1835. [[CrossRef](#)]
9. Xu, Z.; Zheng, B.; Chen, J.; Gao, C. Highly Efficient Synthesis of Neat Graphene Nanoscrolls from Graphene Oxide by Well-Controlled Lyophilization. *Chem. Mater.* **2014**, *26*, 6811–6818. [[CrossRef](#)]
10. Liu, F.; Luo, S.; Liu, D.; Chen, W.; Huang, Y.; Dong, L.; Wang, L. Facile Processing of Free-Standing Polyaniline/SWCNT Film as an Integrated Electrode for Flexible Supercapacitor Application. *ACS Appl. Mater. Interfaces* **2017**, *9*, 33791–33801. [[CrossRef](#)]
11. Akyilmaz, E.; Oyman, G.; Cinar, E.; Odabas, G. A New Polyaniline–Catalase–Glutaraldehyde-Modified Biosensor for Hydrogen Peroxide Detection. *Prep. Biochem. Biotechnol.* **2017**, *47*, 86–93. [[CrossRef](#)]
12. Verma, S.; Das, T.; Pandey, V.K.; Verma, B. Nanoarchitectonics of GO/PANI/CoFe₂O₄ (Graphene oxide/polyaniline/Cobalt Ferrite) based hybrid composite and its use in fabricating symmetric supercapacitor devices. *J. Mol. Struct.* **2022**, *1266*, 133515. [[CrossRef](#)]
13. Zheng, B.; Gao, C. Preparation of Graphene Nanoscroll/Polyaniline Composites and Their Use in High Performance Supercapacitors. *New Carbon Mater.* **2016**, *31*, 315–320. [[CrossRef](#)]
14. Zheng, X.; Ali Mohsin, M.E.; Arsad, A.; Hassan, A. Polymerization of Polyaniline under Various Concentrations of Ammonium Peroxydisulfate and Hydrochloric Acid by Ultrasonic Irradiation. *J. Appl. Polym. Sci.* **2021**, *138*, 50637. [[CrossRef](#)]
15. Cho, S.; Shin, K.-H.; Jang, J. Enhanced Electrochemical Performance of Highly Porous Supercapacitor Electrodes Based on Solution Processed Polyaniline Thin Films. *ACS Appl. Mater. Interfaces* **2013**, *5*, 9186–9193. [[CrossRef](#)] [[PubMed](#)]
16. Wei, X.-L.; Wang, Y.Z.; Long, S.M.; Bobeczko, C.; Epstein, A.J. Synthesis and Physical Properties of Highly Sulfonated Polyaniline. *J. Am. Chem. Soc.* **1996**, *118*, 2545–2555. [[CrossRef](#)]
17. Barbosa, O.; Ortiz, C.; Berenguer-Murcia, Á.; Torres, R.; Rodrigues, R.C.; Fernandez-Lafuente, R. Glutaraldehyde in Bio-Catalysts Design: A Useful Crosslinker and a Versatile Tool in Enzyme Immobilization. *RSC Adv.* **2014**, *4*, 1583–1600. [[CrossRef](#)]
18. Mohan, A.M.V.; Rajendran, V.; Mishra, R.K.; Jayaraman, M. Recent advances and perspectives in sweat based wearable electrochemical sensors. *TrAc Trends Anal. Chem.* **2020**, *131*, 116024. [[CrossRef](#)]
19. Kim, Y.G.; Nguyen, H.L.; Kinlen, P. Secondary dopants of electrically conducting polyaniline. *Polymers* **2021**, *13*, 2904. [[CrossRef](#)]
20. Nagaraja, M.; Mahesh, H.M.; Manjanna, J.; Rajanna, K.; Kurian, M.Z.; Lokesh, S.V. Effect of Multiwall Carbon Nanotubes on Electrical and Structural Properties of Polyaniline. *J. Electron. Mater.* **2012**, *41*, 1882–1885. [[CrossRef](#)]
21. Zhou, Y.; Wang, Y.; He, D.; Ju, C.; Gao, Q.; Gao, L.; Fu, M. Synthesis and Properties of Nano-Polyaniline Films Doped with Camphor Sulfonic Acid. *J. Nanosci. Nanotechnol.* **2014**, *14*, 3417–3421. [[CrossRef](#)] [[PubMed](#)]
22. Jeon, S.S.; Kim, C.; Lee, T.H.; Lee, Y.W.; Do, K.; Ko, J.; Im, S.S. Camphorsulfonic Acid-Doped Polyaniline Transparent Counter Electrode for Dye-Sensitized Solar Cells. *J. Phys. Chem. C* **2012**, *116*, 22743–22748. [[CrossRef](#)]

23. Awata, R.; Shehab, M.; El Tahan, A.; Soliman, M.; Ebrahim, S. High Performance Supercapacitor Based on Camphor Sulfonic Acid Doped Polyaniline/Multiwall Carbon Nanotubes Nanocomposite. *Electrochim. Acta* **2020**, *347*, 136229. [[CrossRef](#)]
24. Qiu, H.; Wang, J.; Qi, S.; He, Z.; Fan, X.; Dong, Y. Microwave Absorbing Properties of Multi-Walled Carbon Nanotubes/Polyaniline Nanocomposites. *J. Mater. Sci. Mater. Electron.* **2015**, *26*, 564–570. [[CrossRef](#)]
25. Cho, S.; Kim, M.; Lee, J.S.; Jang, J. Polypropylene/Polyaniline Nanofiber/Reduced Graphene Oxide Nanocomposite with Enhanced Electrical, Dielectric, and Ferroelectric Properties for a High Energy Density Capacitor. *ACS Appl. Mater. Interfaces* **2015**, *7*, 22301–22314. [[CrossRef](#)]
26. Liu, Y.; Ma, Y.; Guang, S.; Xu, H.; Su, X. Facile Fabrication of Three-Dimensional Highly Ordered Structural Polyaniline–Graphene Bulk Hybrid Materials for High Performance Supercapacitor Electrodes. *J. Mater. Chem. A* **2014**, *2*, 813–823. [[CrossRef](#)]
27. Vilian, A.T.E.; Mani, V.; Chen, S.-M.; Dinesh, B.; Huang, S.-T. The Immobilization of Glucose Oxidase at Manganese Dioxide Particles-Decorated Reduced Graphene Oxide Sheets for the Fabrication of a Glucose Biosensor. *Ind. Eng. Chem. Res.* **2014**, *53*, 15582–15589. [[CrossRef](#)]
28. Bhadra, S.; Khastgir, D.; Singha, N.K.; Lee, J.H. Progress in Preparation, Processing and Applications of Polyaniline. *Prog. Polym. Sci.* **2009**, *34*, 783–810. [[CrossRef](#)]
29. Rahmani, M.; Ghafoori Fard, H.; Ahmadi, M.T.; Rahmani, K. Analytical Prediction of Carbon Nanoscroll-Based Electrochemical Glucose Biosensor Performance. *Int. J. Environ. Anal. Chem.* **2017**, *97*, 1024–1036. [[CrossRef](#)]
30. Meng, L.; Xia, Y.; Liu, W.; Zhang, L.; Zou, P.; Zhang, Y. Hydrogen Microexplosion Synthesis of Platinum Nanoparticles/Nitrogen Doped Graphene Nanoscrolls as New Amperometric Glucose Biosensor. *Electrochim. Acta* **2015**, *152*, 330–337. [[CrossRef](#)]
31. Peng, X.; Meng, L.; Zhang, W.; Liu, W.; Zhang, L.; Zhang, Y. Facile Preparation of Nitrogen-Doped Graphene Scrolls via Acoustic Cavitation as Electrocatalyst for Glucose Biosensing. *J. Solid State Electrochem.* **2016**, *20*, 439–447. [[CrossRef](#)]
32. Ajala, O.; Werther, C.; Mahmudzade, R.; Nikaeen, P.; Depan, D. Crystallization Kinetics of Poly(Lactic Acid)–Graphene Nanoscroll Nanocomposites: Role of Tubular, Planar, and Scrolled Carbon Nanoparticles. *C* **2021**, *7*, 75. [[CrossRef](#)]
33. Li, H.; Papadakis, R.; Jafri, S.H.M.; Thersleff, T.; Michler, J.; Ottosson, H.; Leifer, K. Superior Adhesion of Graphene Nanoscrolls. *Commun. Phys.* **2018**, *1*, 44. [[CrossRef](#)]
34. Chen, P.-Y.; Hung, H.-L.; Han, C.-C.; Chiu, H.-C. Correlation between Nanoscale Elasticity, Semiconductivity, and Structural Order in Functionalized Polyaniline Thin Films. *Langmuir* **2020**, *36*, 4153–4164. [[CrossRef](#)] [[PubMed](#)]
35. Elnaggar, E.M.; Kabel, K.I.; Farag, A.A.; Al-Gamal, A.G. Comparative Study on Doping of Polyaniline with Graphene and Multi-Walled Carbon Nanotubes. *J. Nanostruct. Chem.* **2017**, *7*, 75–83. [[CrossRef](#)]
36. Li, H.; Liang, Y.; Liu, Y.; Liu, S.; Li, P.; He, C. Engineering Doping Level for Enhanced Thermoelectric Performance of Carbon Nanotubes/Polyaniline Composites. *Compos. Sci. Technol.* **2021**, *210*, 108797. [[CrossRef](#)]
37. Mergen, Ö.B.; Umut, E.; Arda, E.; Kara, S. A Comparative Study on the AC/DC Conductivity, Dielectric and Optical Properties of Polystyrene/Graphene Nanoplatelets (PS/GNP) and Multi-Walled Carbon Nanotube (PS/MWCNT) Nanocomposites. *Polym. Test.* **2020**, *90*, 106682. [[CrossRef](#)]